Geomechanics and Engineering, *Vol. 19, No. 3 (2019) 269-282*
DOI: https://doi.org/10.12989/gae.2019.19.3.269

Numerical simulation on strata behaviours of TCCWF influenced by coal-rock combined body

Zhanbo Cheng[1,2,3], Weidong Pan*[1,2], Xinyuan Li[1,2] and Wenbin Sun[4]

[1]*School of Energy and Mining Engineering, China University of Mining and Technology-Beijing, Beijing 100083, China*
[2]*Coal Industry Engineering Research Center of Top-coal Caving Mining, Beijing 100083, China*
[3]*School of Engineering, University of Warwick, Coventry CV47AL, U.K.*
[4]*College of Mining and Safety Engineering, Shandong University of Science and Technology, Shandong 266590, China*

(Received July 8, 2019, Revised October 20, 2019, Accepted October 22, 2019)

Abstract. Due to top-coal and immediate roof as cushion layer connecting with support and overlying strata, it can make significant influence on strata behaviors in fully mechanical top-coal caving working face (TCCWF). Taking Qingdong 828 working face as engineering background, FLAC^{3D} and UDEC^{2D} were adopted to explore the influence of top-coal thickness (TCT), immediate roof thickness (IRT), top-coal elastic modulus (TCEM) and immediate roof elastic modulus (IREM) on the vertical stress and vertical subsidence of roof, caving distance, and support resistance. The results show that the maximum roof subsidence increases with the increase of TCT and IRT as well as the decrease of TCEM and IREM, which is totally opposite to vertical stress in roof-control distance. Moreover, although the increase of TCEM and IREM leading to the increase of peak value of abutment pressure, the position and distribution range have no significant change. Under the condition of initial weighting occurrence, support resistance has negative and positive relationship with physical parameters (e.g., TCT and IRT) and mechanical properties (e.g., TCEM and IREM), respectively.

Keywords: coal-rock combined body; fully mechanized top-coal caving face; overlying strata behavior; numerical simulation

1. Introduction

As shown in Fig. 1, China is the largest producer and consumer of coal in the World, who accounts to about half of the total coal production and consumption of the World, especially in recent years (BP, 2018). In the explored coal seam storage, the thick coal seam (thickness ≥3.5 m) in China is rich in reserves and production accounting for about 45% of the total coal seam reserves and production (Wang *et al.* 2015, Zhang *et al.* 2019, Sun *et al.* 2019, Kong *et al.* 2019, Liu and Cheng 2019, Liu *et al.* 2018, Lv *et al.* 2019, Cheng *et al.* 2018, 2019). Thus, it plays a significant role in the performance of Chinese coal industry (Wang *et al.* 2014). At present, there are three methods of multi-slice mining, large cutting height mining and top-coal caving mining adopted in thick coal seam mining and the production methods are generally similar at the former Yugoslavia, Hungary, Poland, France, India and China (Alehossein and Poulsen 2010, Schweitzer 1977, Suchowerska *et al.* 2015). Top-coal caving mining is cost effective because the major features is the lower part of a coal seam cutting with 2-3 m height, followed by drawing of the broken top-coal to allow the upper part crushed into fragments under the overburden pressure and drawn through an opening at the rear of the shield support. The broken top-coal finally is caved under gravity directly on, and removed from the face by, the armored chain conveyor behind (Wang *et al.* 2014, Alehossein and Poulsen 2010). Moreover, it can achieve high efficiency and effective production of coal, reduce the quantities of roadway excavation and the number of workfaces moving, decrease material consumption under complex geological conditions and coal seam occurrence conditions (e.g., steep inclined thick coal seam). Therefore, top-coal caving mining occupies is one of the major mining methods for extracting thick coal seams (Basarir *et al.* 2015, Wang 2018, Wang *et al.* 2014, Alehossein and Korinets 2000, Hoek and Brown 1997).

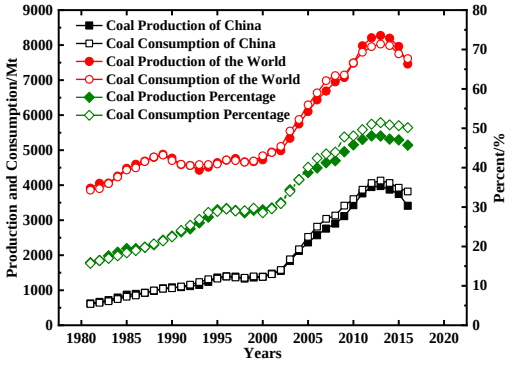

Fig. 1 Coal production and consumption of China and the World

In terms of using numerical simulation to study top-coal

*Corresponding author, Associate Professor
E-mail: pwd@cumtb.edu.cn

ISSN: 2005-307X (Print), 2092-6219 (Online)

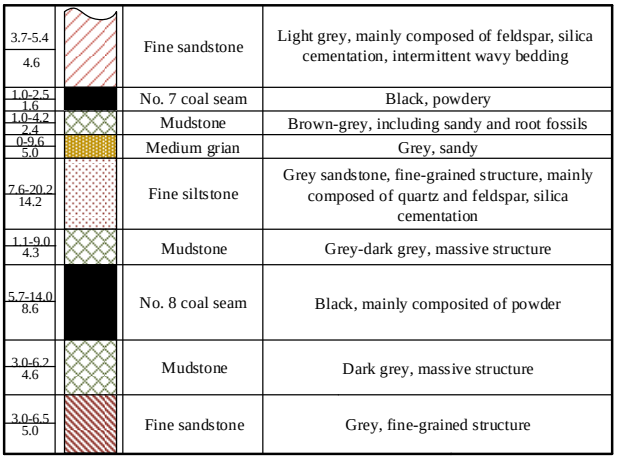

Fig. 2 Comprehensive stratigraphic column of 828 working face

Table 1 Basic mechanical parameters of coal and rock mass in 828 working face

No.	Layer name	Thickness (m)	Bulk density (kN/m3)	Bulk modulus (GPa)	Shear modulus (GPa)	Internal friction angle (°)	Cohesion (MPa)	Tensile strength (MPa)
12	Fine sandstone	4.6	25.9	3.65	2.62	35	2.8	1.7
11	No.7coal seam	1.6	14	2.67	1.60	25	1.5	0.8
10	Mudstone	2.4	26.4	3.15	2.07	27	2.0	1.0
9	Medium grain	5.0	24.2	3.42	2.21	30	2.2	1.4
8	Fine siltstone	14.2	30	6.5	4.88	39	8	4.5
7	Mudstone	4.3	26.4	3.15	2.07	27	2.0	1.0
6	No.8 coal seam	8.6	13	2.43	1.39	25	1.5	0.8
5	Mudstone	4.6	26.4	3.15	2.07	27	2.0	1.0
4	Siltstone	5.0	26	4.14	2.98	35	3.2	2.0
3	Mudstone	5.0	26.4	3.15	2.07	27	2.0	1.0
2	Medium grain	10	24.2	3.42	2.21	30	2.2	1.4
1	Fine sandstone	15	25.9	3.65	2.62	35	2.8	1.7

caving mining method, Xie *et al.* (1999) obtained the distribution of the abutment pressure and the deformation and failure of top-coal in mining process through numerical simulations by using FLAC software. Moreover, a macro-shell composed of high stress existed in the rock surrounding an TCCWF, which is higher than its external and internal stresses through numerical and physical modeling tests (Xie *et al.* 2009). And the stress shell acts as the primary support system of forces due to bear and transfer the loads of overlying strata. Therefore, TCCWF was situated within the lower-stress zone and the mechanical nature of top-coal acting as a cushion layer was revealed. Alehossein and Poulsen (2010) developed a yield function to aid in the assessment of TCCWF by considering the in situ geological, geometrical and geotechnical conditions and the trends predicted by the yield function and the option of considering other geotechnical variables were confirmed by numerical modelling. On the other hand, researchers focus on how to increase the top-coal recovery ratio. Taken Omerler Underground Mine located at Turkey as engineering background, Yasitli and Unver (2005) illustrated top-coal should be uniformly fractured for decreasing dilution and increasing extraction ratio and efficiency of operation. Xie and Zhao (2009) demonstrated a new theory with vibration to increase top-coal recovery ratio by using discrete element method and the arch structure can be formed easily on the performance of vibration during the top-coal caving process. Wang *et al.* (2014) illustrated the recovery of top-coal affected by the thickness of top-coal, drawing technique and parameters. And the 3D draw body of top-coal resembles an approximate ellipsoid by numerical modelling.

However, there are limit references to describe the overlying strata behaviors of considering the top-coal and immediate roof as a combined body. Therefore, the aims of this paper are to analyze the properties of cushion layer (TCT, IRT, TCEM and IREM) how to influence overlying strata behaviors (vertical stress, roof subsidence, first weighting interval and support resistance) by using numerical simulations.

2. Engineering background

Qingdong coal mine is in the location of Huaibei Municipality, Anhui Province, China. 828 mining face of

No. 8 coal seam was adopted top-coal caving method. And the average thickness of this working face is 8.6 m along with the cut mining height 2.5 m. It has a buried depth ranging from 475 to 520 m and inclined angle ranging from 5 to 18°. Comprehensive stratigraphic column of 828 working face is shown in Fig. 2 and Table 1 shows the corresponding physical and mechanical parameters of each layer.

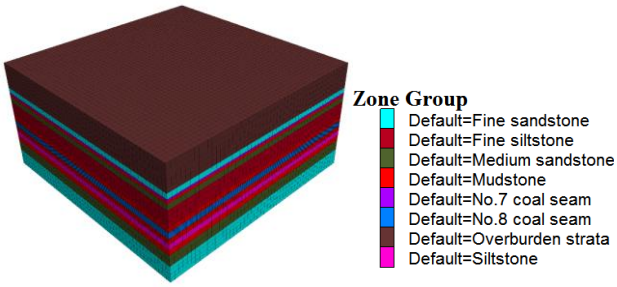

Fig. 3 Numerical model

3. Numerical simulation by using FLAC^{3D}

3.1 Yield strength criterion

It is of great importance to select a reasonable constitutive model in numerical simulation (Itasca Consulting Group 2012). In general, coal body occurrences failure and plastic movement after load reaching to the ultimate strength of rock. At the same time, the residual strength of rock can be observed a significant decreasing. Therefore, Mohr-Coulomb criterion is adopted as estimating the failure of coal and rock bodies. The expression of stress-strain can be shown as follows

$$f_s = \sigma_1 - \sigma_3 \frac{1+\sin\varphi}{1-\sin\varphi} - 2c\sqrt{\frac{1+\sin\varphi}{1-\sin\varphi}} \quad (1)$$

where σ_1 and σ_3 are the maximum principle stress and minimum principle stress, respectively. φ and c are internal friction angle and cohesive, respectively.

Coal and rock bodies generally can be observed the characteristics of resisting compression rather than tensile which means the tensile strength of coal and rock bodies very small. Therefore, coal and rock bodies observe tensile failure when the minimum principle stress is greater than the tensile strength of coal and rock bodies.

3.2 Model establishment

Taking Qingdong 828 working face as engineering background, the numerical model is established by using FLAC^{3D} along with the advancing distance 200 m, inclining distances 200 m and height 100 m, respectively, as shown in Fig. 3. This model includes No.7 and No.8 coal seam along with its roof and floor. It should be noted that 828 working face is extracting No.8 coal seam with the thickness of 8.6 m. And the immediate roof and main roof of No.8 coal seam are 4.3 m and 14.2 m, respectively. The horizontal displacement on both sides are restricted and vertical displacement on bottom side is restricted as well. Moreover, top surface is applied with the vertical stress of -1.18×107 Pa to simulate the self-weight of overlying strata. Without considering tectonic stress, the horizontal stress is 0.3 times of vertical stress equaling to 3.54×106 Pa. And the adopt physical and mechanical parameter of numerical simulation are listed as Table 1.

3.3 Simulation results

For analyzing the influence of coal-rock combined body on overlying strata behaviors, the change laws of vertical displacement and stress of roof can be observed through changing TCT, IRT, TCEM and IREM.

3.3.1 Top-coal thickness

TCT is adopted with 3 m, 6 m, 9 m and 12 m and other mechanical parameters of coal and rock bodies keep constant to explore the laws of roof subsidence and vertical stress. The change laws of roof subsidence with the increase of TCT are shown in Fig. 4.

Five specimens were measured and calculated to obtain the average value in order to ensure the accuracy of result in same temperature and moisture content. The WAW-600B micro-computer controlled electro hydraulic servo universal testing machine was used in this study as shown in Fig. 5. It is mainly composed of the following parts: 600kN axial actuator, axial load and displacement transducers, screen display and testing results treatment. The device can be regarded as a rigid test machine because the failure strengths of the frozen soil are very small in relation to the measurement range of the test apparatus. Therefore, it meets the requirement of the International Society for Rock Mechanics (Hatheway 2009). During the experimental loading process, the strain rate used for all the specimens was 10 mm/min to make sure the loading time was around 2 minutes only. At the same time, heat insulated foam plates were wrapped around the upper and lower loading plates for ensuring the temperature of specimens remaining constant, too.

It reflects the conditions of vertical displacement under the same advancing distance with various TCT. To be specific, the maximum subsidence is 0.115 m, 0.213 m, 0.767 m and 0.827 m when TCT is 3 m, 6 m, 9 m and 12 m, respectively. Obviously, the maximum subsidence increases with the increase of TCT. For analysing the change of TCT influencing on the deformation of overlying strata in roof-control distance, taking below of main roof with 1m from the rear of support 5 m, 3 m and 0 m (coal wall) as monitoring points, it can be concluded that the roof subsidence gradually decreases with the advancing direction and the limit change can be observed. Moreover, the roof subsidence almost linearly increases with the increase of TCT under the same location.

On the other hand, vertical stress versus TCT can be illustrated as Fig. 5. The maximum stress is 25.91 MPa, 30.91 MPa, 32.41 MPa and 34.98 MPa when TCT is 3 m, 6 m, 9 m and 12 m, respectively. The increase of TCT causes the maximum supporting pressure in advance of working face increasing and forward move of peak point. Therefore, the advancing pressure is distributed widely. For analysing

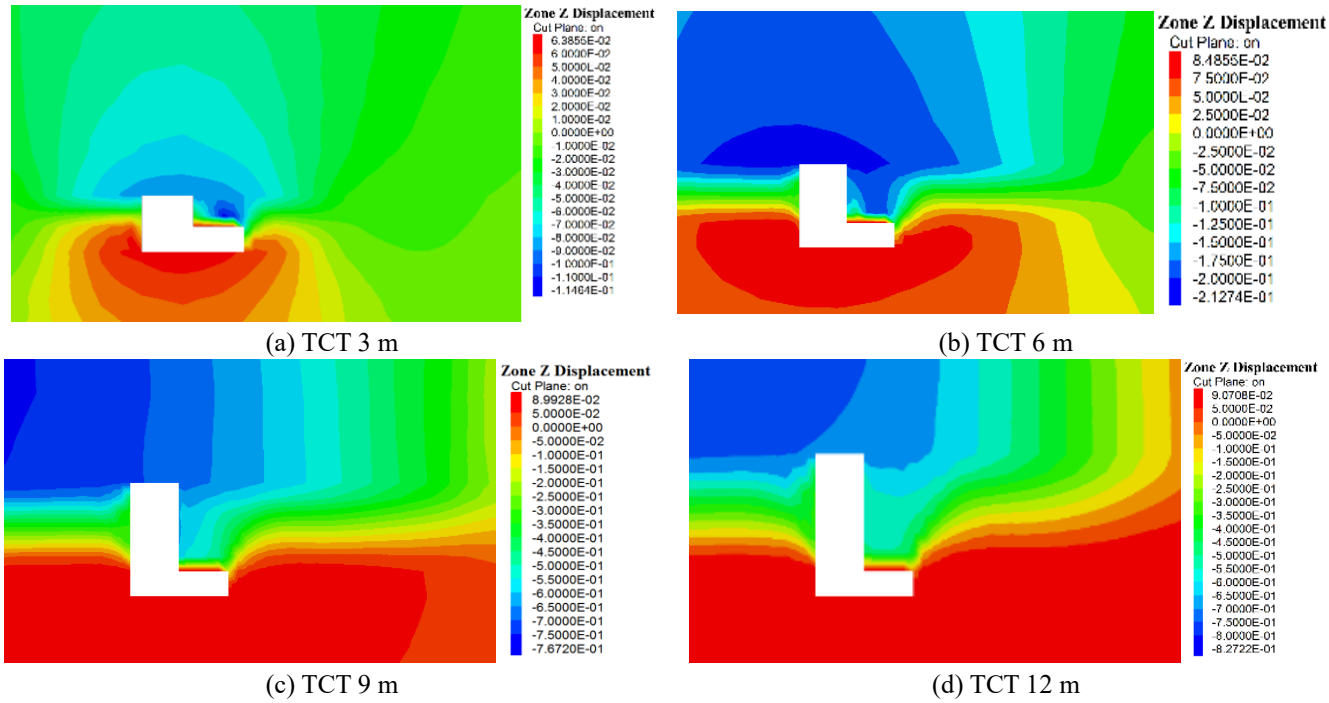

(a) TCT 3 m (b) TCT 6 m

(c) TCT 9 m (d) TCT 12 m

Fig. 4 Displacement nephogram versus TCT

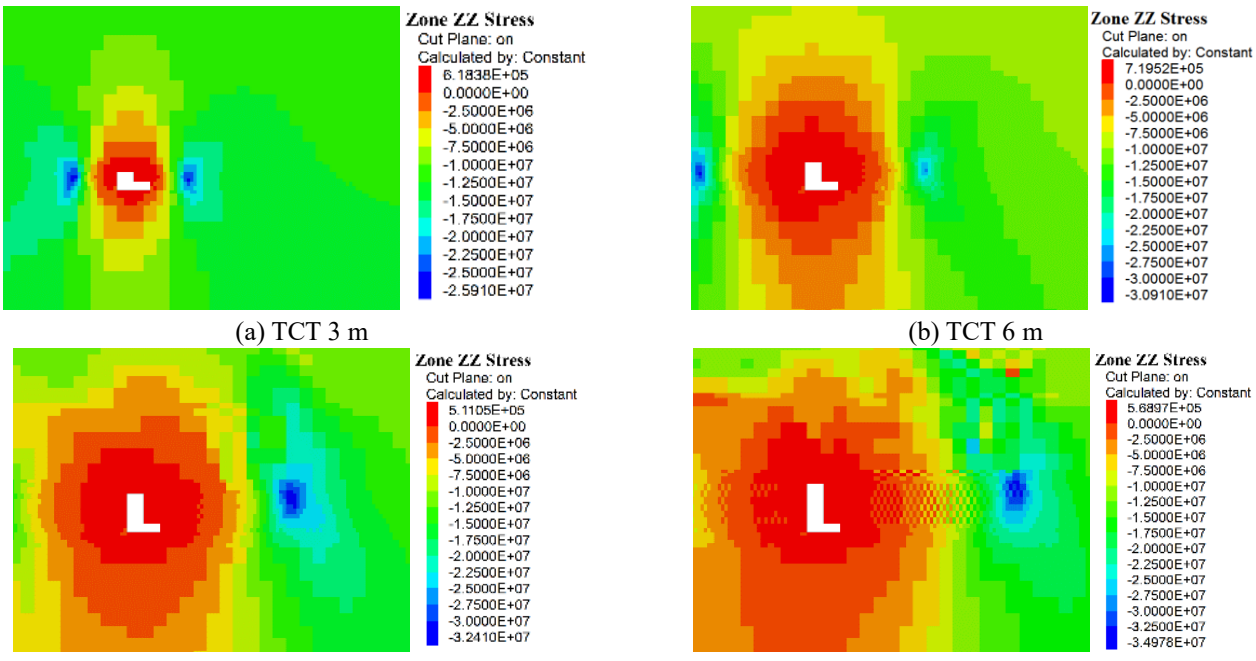

(a) TCT 3 m (b) TCT 6 m

(c) TCT 9 m (d) TCT 12 m

Fig. 5 Stress nephogram versus TCT

TCT influencing on roof stress within the roof-control distance, the location of interface between fine silt and mudstone is selected. With the increase of TCT, vertical stress decreases from 900 kPa to 150 kPa with its tendency gradually to slow.

3.3.2 Immediate roof thickness

IRTs are selecting as 3 m, 5 m, 7 m and 9 m to analyse the results of vertical stress and vertical displacement on TCCWF. The details as follows.

Fig. 6 reflects the vertical displacement with various IRTs and same advancing distance. To be specific, the maximum vertical displacement is 0.176 m, 0.185 m, 0.194 m and 0.200 m when IRT is 3 m, 5 m, 7 m and 9 m, respectively. It can be observed that IRT has no significant influence on the maximum vertical displacement. In terms of a specific point, the vertical displacement linear increases with the increase of IRT due to the mining space dramatically increasing. Moreover, the vertical displacement gradually decreases along with the advancing

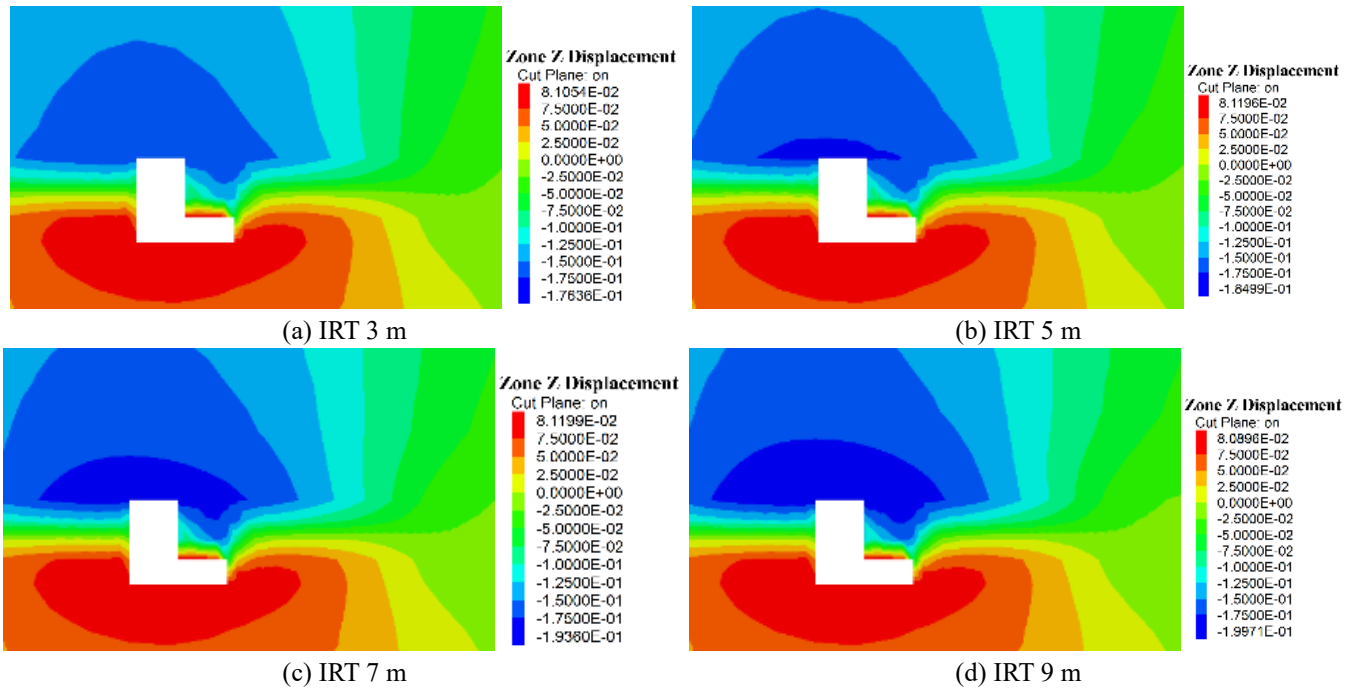

(a) IRT 3 m (b) IRT 5 m

(c) IRT 7 m (d) IRT 9 m

Fig. 6 Displacement nephogram versus IRT

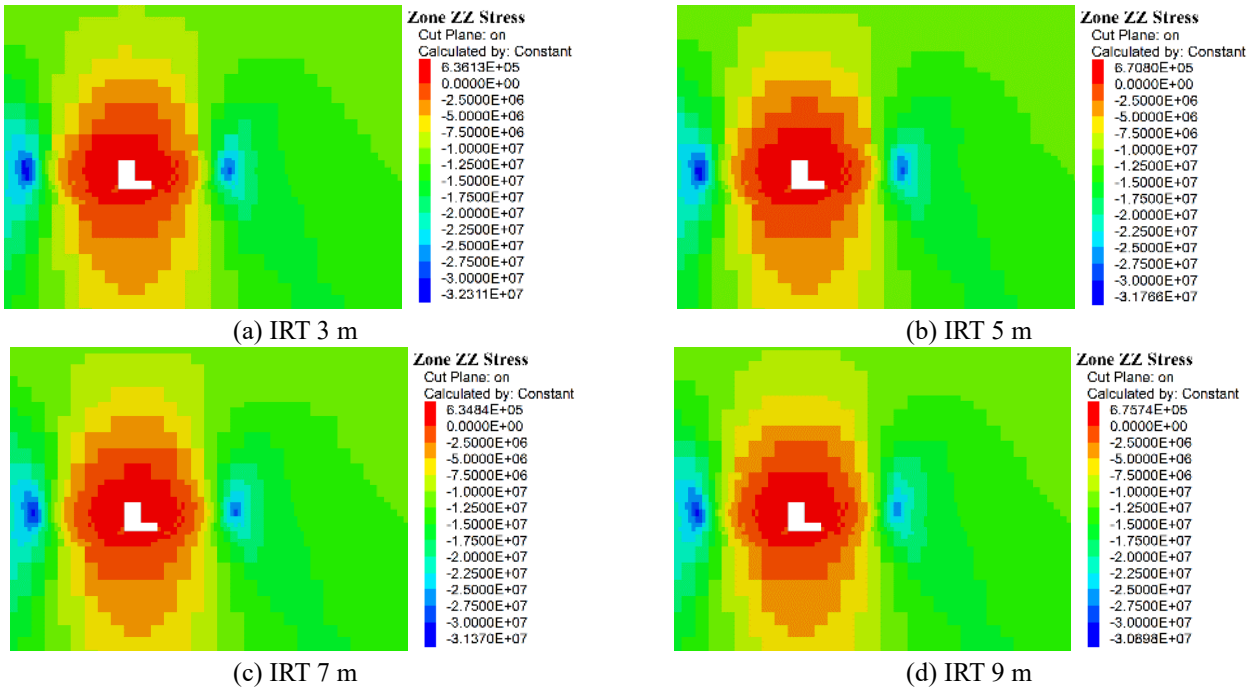

(a) IRT 3 m (b) IRT 5 m

(c) IRT 7 m (d) IRT 9 m

Fig. 7 Stress nephogram versus IRT

direction in the limit roof-control range. Therefore, the maximum and minimum vertical displacement of main roof can be observed in the location of goaf and coal wall, respectively.

In terms of vertical stress as shown in Fig. 7, the maximum value is 32.31 MPa, 31.78 MPa, 31.37 MPa and 30.90 MPa when IRT is 3 m, 5 m, 7 m and 9 m, respectively. The maximum support pressure obviously decreases with the increase of IRT, while the location of peak point has no change. Therefore, IRT has influence on peak value rather than stress distribution. For a specific point, the vertical stress gradually decreases with the increase of IRT along with a slow decrement as well.

3.3.3 Top-coal elastic modulus

Obviously, TCEM has significant influence on vertical stress and displacement. Therefore, keeping mining height, TCT, IRT and other mechanical properties constant, TCEMs with 1.15 GPa, 1.72 GPa, 3.29 GPa and 4.42 GPa are selected to explore vertical stress and displacement. The details are illustrated as follows.

As shown in Fig. 8, the maximum roof subsidence is

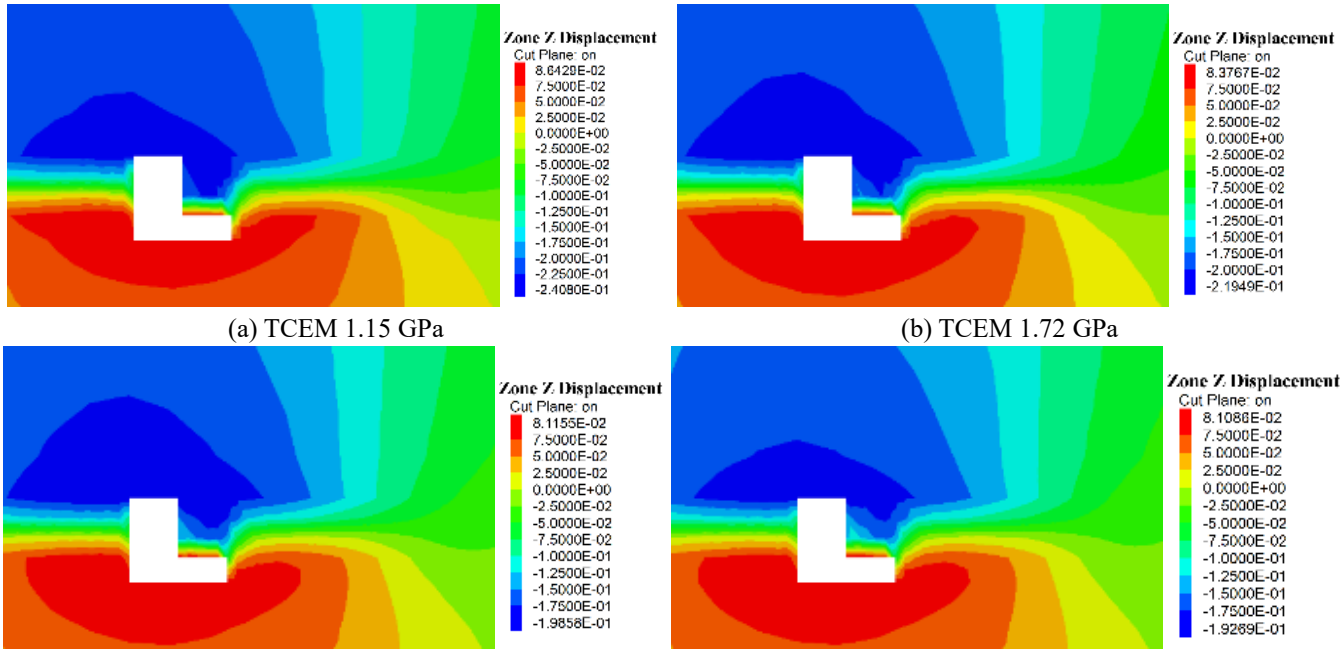

(a) TCEM 1.15 GPa (b) TCEM 1.72 GPa

(c) TCEM 3.29 GPa (d) TCEM 4.42 GPa

Fig. 8 Displacement nephogram versus TCEM

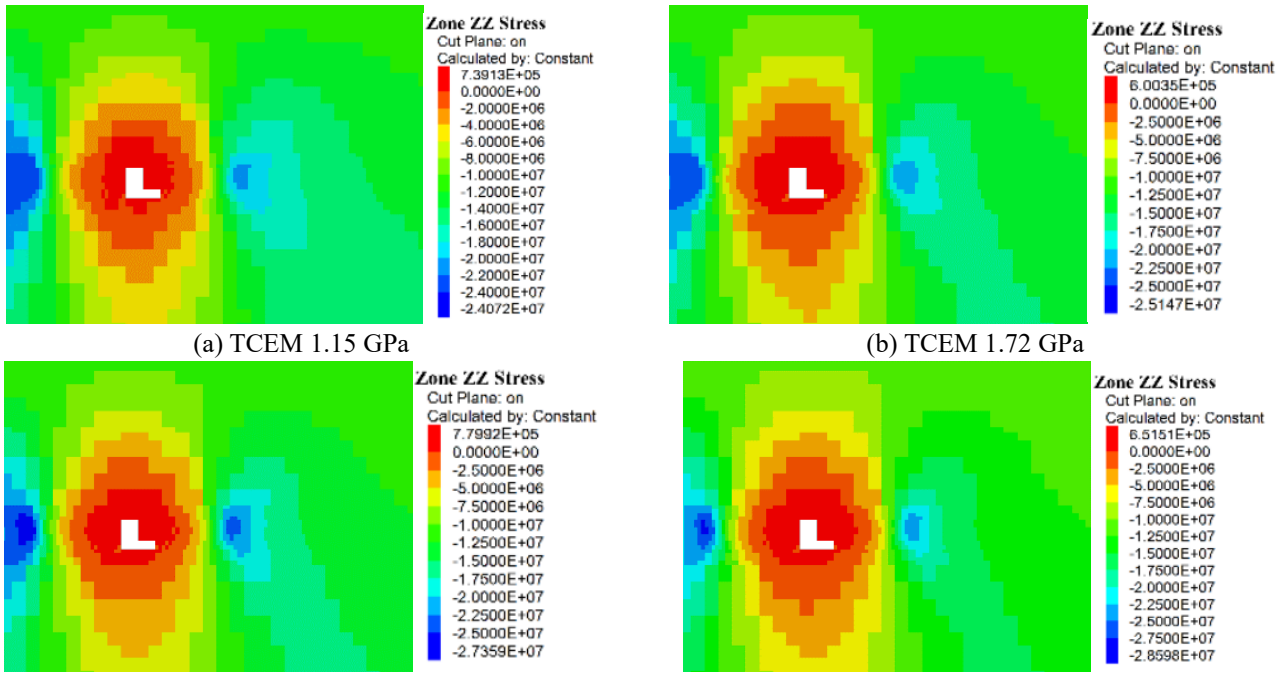

(a) TCEM 1.15 GPa (b) TCEM 1.72 GPa

(c) TCEM 3.29 GPa (d) TCEM 4.42 GPa

Fig. 9 Stress nephogram versus TCEM

0.241 m, 0.219 m, 0.199 m and 0.193 m with TCEM of 1.15 GPa, 1.72 GPa, 3.29 GPa and 4.42 GPa, respectively. The higher TCEM possesses higher compressive strength representing the better integrity of top-coal. Therefore, the mechanical properties of coal-rock combined body is better to undertake the load of overlaying strata causing less roof subsidence.

In terms of a specific point, the vertical displacement decreases with the increase of TCEM. In the limit range of roof-control, roof subsidence decreases along with advancing direction. That means the minimum roof subsidence can be observed in the location of coal wall.

The maximum stress is 24.07 MPa, 25.15 MPa, 27.36 MPa and 28.60 MPa under four conditions with the increase of TCEM as shown in Fig. 9. However, the peak point of advancing support stress increases with the increase of TCEM, while the change of TCEM has no influence on the stress distribution. Taking the interface of fine siltstone and mudstone as a specific cross-section, the vertical stress increases with the increase of TCEM for any point in this cross-section.

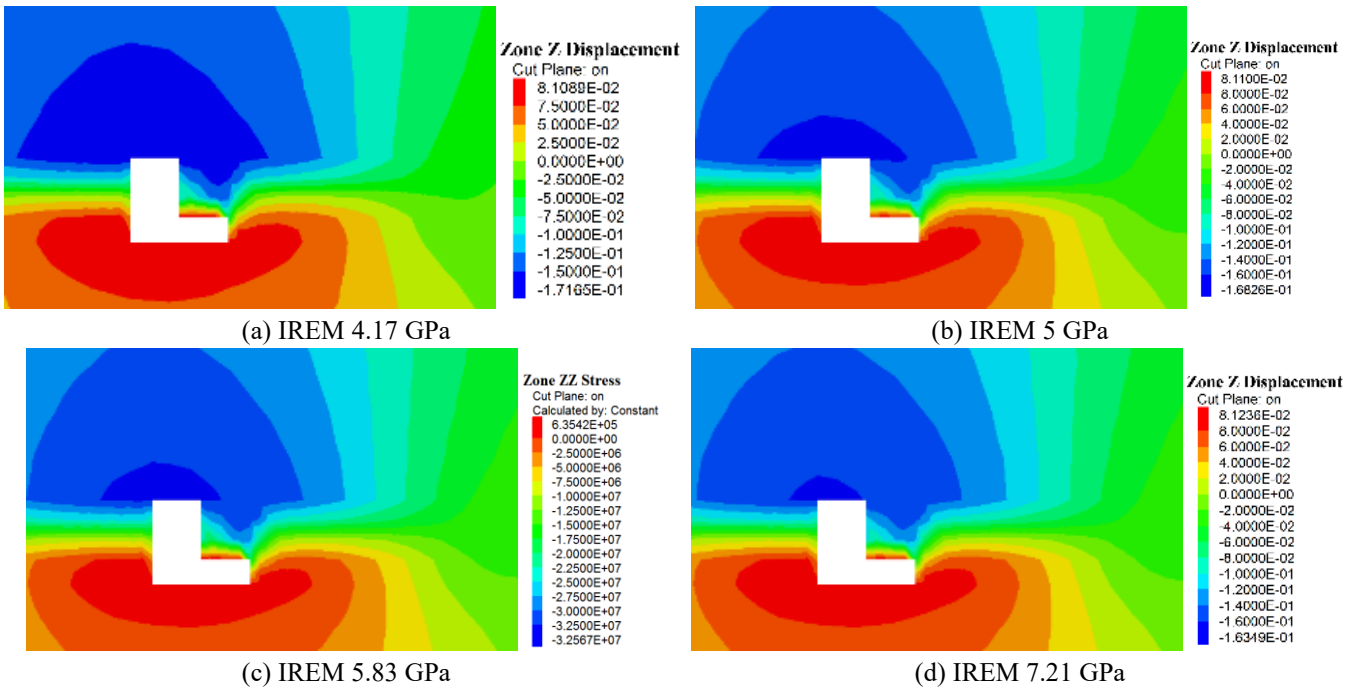

(a) IREM 4.17 GPa (b) IREM 5 GPa

(c) IREM 5.83 GPa (d) IREM 7.21 GPa

Fig. 10 Displacement nephogram versus TCEM

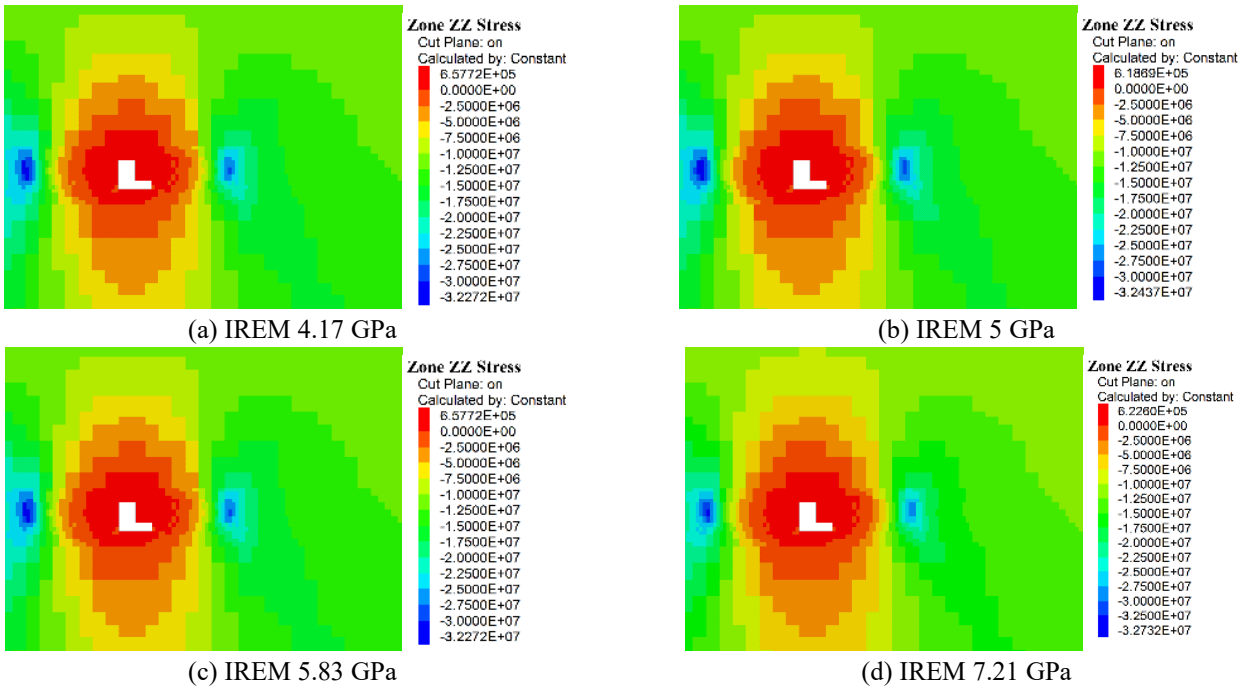

(a) IREM 4.17 GPa (b) IREM 5 GPa

(c) IREM 5.83 GPa (d) IREM 7.21 GPa

Fig. 11 Stress nephogram versus TCEM

3.3.4 Immediate roof elastic modulus

The IREM values of 4.17 GPa, 5 GPa, 5.83 GPa and 7.21 GPa are selected to explore the situations of vertical stress and displacement with keeping other mechanical properties constant.

Fig. 10 illustrates the distribution of vertical stress with various IREMs. The maximum roof subsidence is 0.172 m, 0.168 m, 0.166 m and 0.163 m under four conditions with the increase of IREM, respectively. The higher IREM leads to a higher elastic modulus of coal-rock combined body to undertake better bearing capacity. In terms of a specific point, vertical displacement decreases with the increase of IREM and roof subsidence gradually decreases along with the advancing distance under the same horizontal section and the same IREM.

In terms of vertical stress, the maximum value is 32.27 MPa, 32.44 MPa, 32.57 MPa and 32.73 MPa under four conditions with the increase of IREM as shown in Fig. 11. The peak value of advancing support stress increases with the increase of IREM and the location of peak point has no change causing the influence range of advancing support stress keeping constant. Moreover, the vertical stress

increases with the increase of IREM and the increment tends to slow.

4. Numerical simulation by using UDEC^{2D}

4.1 Design schemes

Taking Qingdong 828 working face as engineering background, overlying strata behaviors (e.g., initial caving distance, periodic caving distance, roof subsidence and support loading) are explored with various conditions (TCT, IRT, TCEM and IREM) of coal-rock combined body.

In this numerical simulation, plane-strain model is adopted (Itasca Consulting Group 2004). The length, width and mining height are 100 m, 100m and 2.5 m, respectively, as shown in Fig. 12. The upper boundary is uniform load and both sides are restricted in horizontal direction. Moreover, the lower boundary is restricted in vertical displacement. And the gravitational acceleration is 9.8 m/s^2.

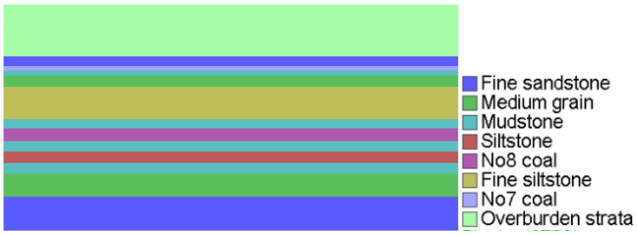

Fig.12 Numerical model

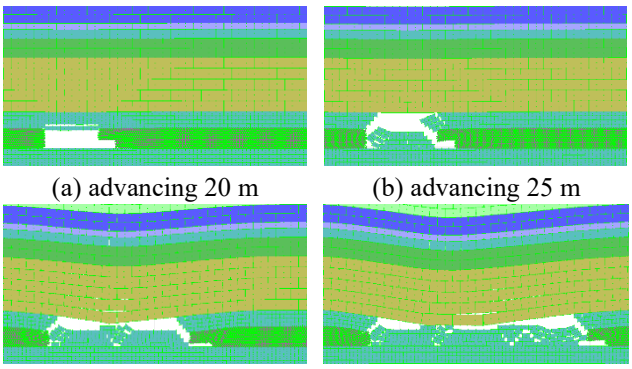

(a) advancing 20 m (b) advancing 25 m

(c) advancing 45 m (d) advancing 65 m

Fig.13 Top-coal thickness 3 m

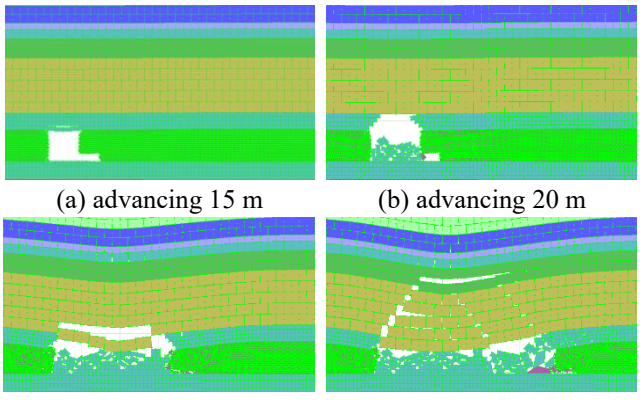

(a) advancing 15 m (b) advancing 20 m

(c) advancing 40 m (d) advancing 55 m

Fig.14 Top-coal thickness 6 m

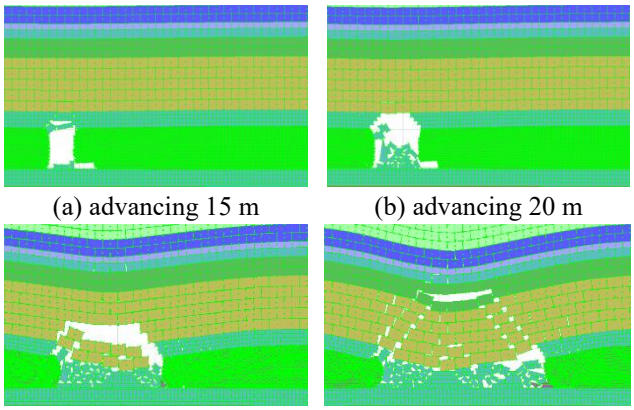

(a) advancing 15 m (b) advancing 20 m

(c) advancing 40 m (d) advancing 55 m

Fig.15 Top-coal thickness 9 m

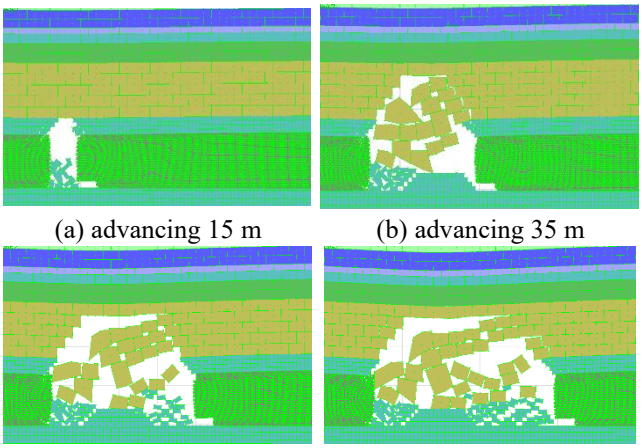

(a) advancing 15 m (b) advancing 35 m

(c) advancing 45 m (d) advancing 55 m

Fig. 16 Top-coal thickness 12 m

For analyzing the influence of TCT, IRT, TCEM and IREM on caving distance, roof subsidence and support resistance, TCTs are selecting as 3 m, 6 m, 9 m and 12 m, IRTs are selecting as 3 m, 5 m, 7 m and 9 m, TCEMs are selecting as 1.15 GPa, 1.72 GPa, 3.29 GPa and 4.42 GPa, IREMs are selecting as 4.17 GPa, 5.00 GPa, 5.83 GPa and 7.21 GPa, to explore the overlying strata behaviors in Qingdong 828 working face.

4.2 Simulation results

4.2.1 Top-coal thickness

Figs. 13-15 illustrate the strata behaviors under different TCT. As shown in Fig. 13, immediate roof has obviously separation layer with advancing distance of 20 m when TCT is 3 m. Subsequently, immediate roof collapses directly when advancing distance is 25 m. And initial caving weight can be observed with the working face continue to advance reaching to 45 m. Moreover, the first periodic caving weight can be observed in the advancing distance of 65 m. It can be concluded that the initial caving distance and periodic caving distance are 45 m and 20 m, respectively, when TCT is 3 m.

The obviously separation layer and initial collapsing of immediate roof can be observed when the advancing distance is 15 m and 20 m, respectively, with TCT of 6 m.

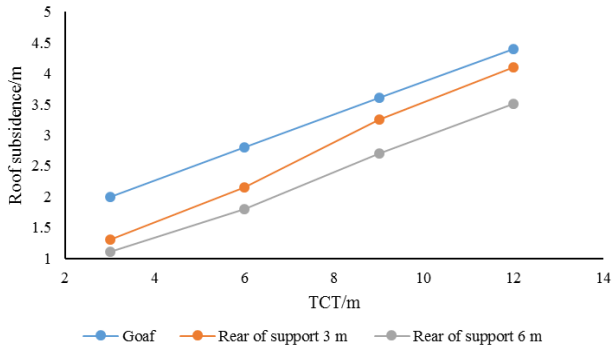

(a) Roof subsidence under initial caving

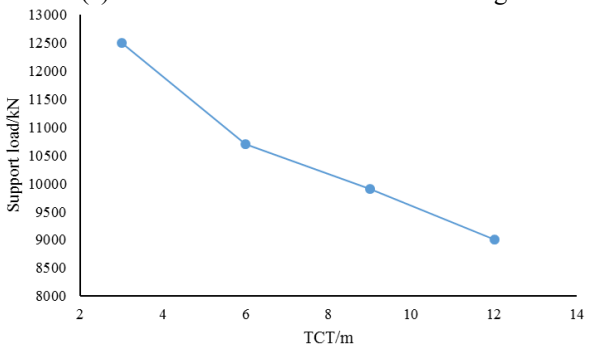

(b) Support load under initial caving

Fig.17 Characteristics of initial weighting versus TCT

Subsequently, the initial caving distance and periodic caving distance can be obtained with the advancing distance of 40 m and 55 m, respectively. Therefore, the initial caving distance and periodic caving distance are 40 m and 15 m, respectively, as shown in Fig. 14.

Fig. 15 illustrates the strata behaviors when TCT is 9 m. The initial caving of immediate roof and main roof is occurred in the advancing distance of 20 m and 40 m, respectively. Subsequently, the first and second periodic caving weight can be observed in the advancing distance of 55 m and 65 m, respectively. Initial caving distance and periodic caving distance are 40 m and 10-15 m, respectively. With the increase of TCT, mining space increases as well causing the decrease of caving distance.

Fig. 16 illustrates the strata behaviors when TCT is 12 m. The initial caving of immediate roof and main roof is occurred in the advancing distance of 15 m and 35 m, respectively. Subsequently, the first and second periodic caving weight can be observed in the advancing distance of 45 m and 55 m, respectively. Initial caving distance and periodic caving distance are 35 m and 10 m, respectively. With the increase of TCT, mining space increases as well causing the decrease of caving distance.

Roof subsidence and support load with various TCT are monitored under the occurrence of initial caving weight and the results are shown in Fig. 17. Selecting three positions (goaf, rear of support 3 m, rear of support 5 m) within the range of roof-control distance, roof subsidence almost linear increases with the increase of TCT. And roof subsidence decreases along with the advancing direction within the range of roof-control distance. Support resistance decreases with the increase of TCT and its increment tends to small under the occurrence of initial caving weight.

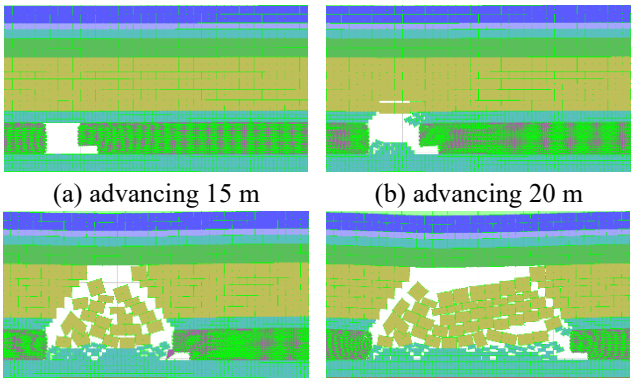

(a) advancing 15 m (b) advancing 20 m

(c) advancing 40 m (d) advancing 60 m

Fig.18 Immediate roof thickness 3 m

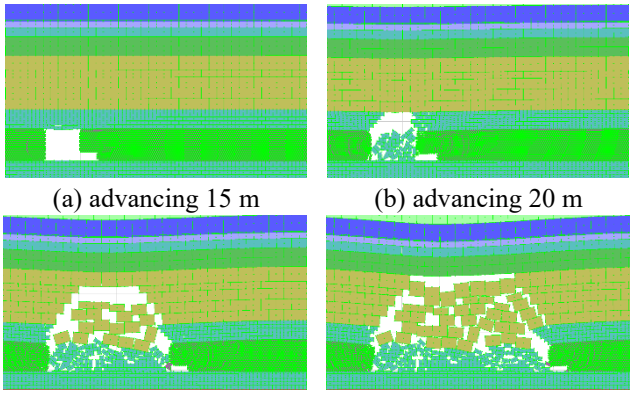

(a) advancing 15 m (b) advancing 20 m

(c) advancing 40 m (d) advancing 55 m

Fig.19 Immediate roof thickness 5 m

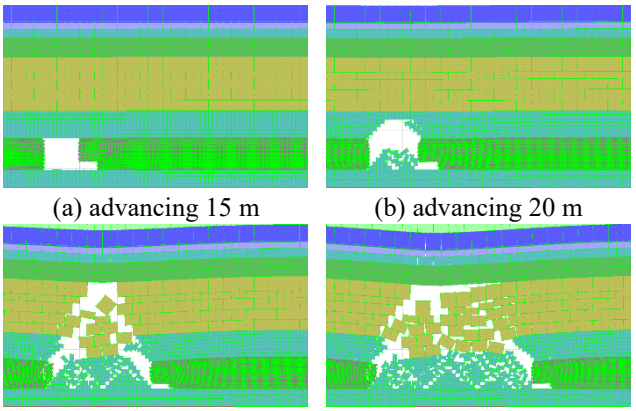

(a) advancing 15 m (b) advancing 20 m

(c) advancing 35 m (d) advancing 50 m

Fig.20 Immediate roof thickness 7 m

4.2.2 Immediate roof thickness

The strata behaviors with various IRT are illustrated in Fig. 18-21. As shown in Fig. 18, there is slightly subsidence of immediate roof when IRT is 3 m. And initial caving of immediate roof is in the advancing distance of 20 m. Moreover, the advancing distance of 40 m occurs initial caving of main roof. And with the advancing distance continually reaching to 60 m, the first periodic caving weight can be occurred. Therefore, the initial caving distance and periodic caving distance are 40 m and 20 m, respectively, when IRT is 3 m.

A significant separation layer can be observed when

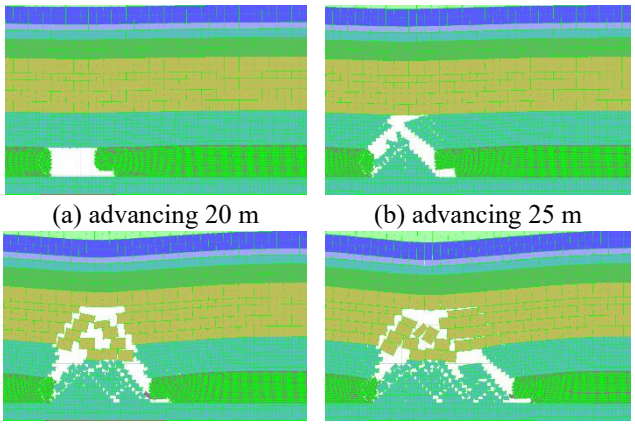

(a) advancing 20 m (b) advancing 25 m

(c) advancing 35 m (d) advancing 45 m

Fig. 21 Immediate roof thickness 9 m

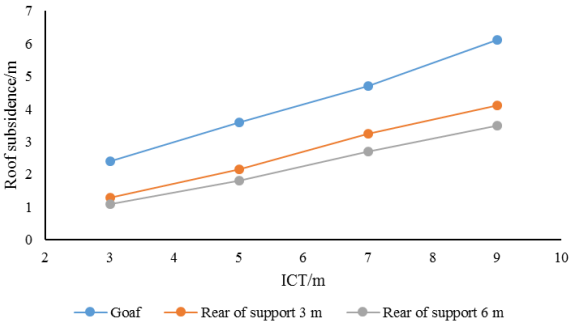

(a) Roof subsidence under initial caving

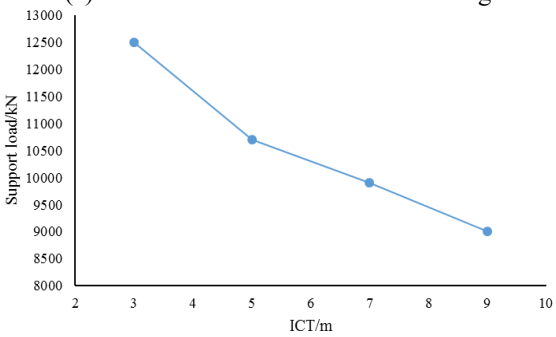

(b) Support load under initial caving

Fig. 22 Characteristics of initial weighting versus IRT

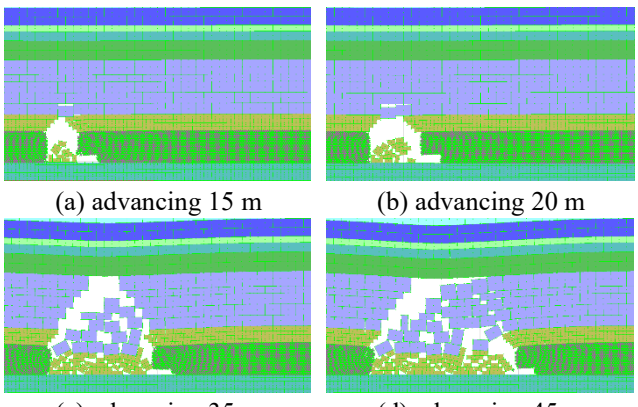

(a) advancing 15 m (b) advancing 20 m

(c) advancing 35 m (d) advancing 45 m

Fig. 23 Top-coal elastic modulus 1.15 GPa

working face is advanced in 15 m under IRT of 5 m as shown in Fig. 19. Initial caving distance of immediate roof and main roof is 20 m and 40 m, respectively. With working face continue to reach to 55 m, the first periodic weight can be observed. Therefore, the initial caving distance and periodic caving distances are 40 m and 15 m, respectively, with IRT of 5 m.

As shown in Fig. 20, the initial caving weight can be observed when the advancing distance is 35 m. And another 15 m advancing leads to the first periodic caving weight. Therefore, the initial caving distance and periodic caving distance can be regards as 35 m and 15 m with the IRT of 7 m.

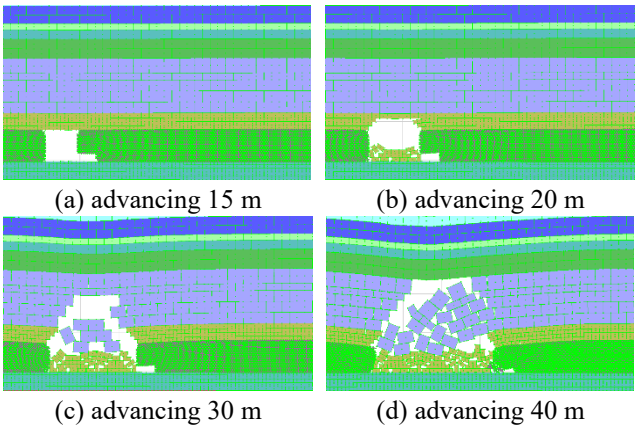

(a) advancing 15 m (b) advancing 20 m

(c) advancing 30 m (d) advancing 40 m

Fig. 24 Top-coal elastic modulus 1.72 GPa

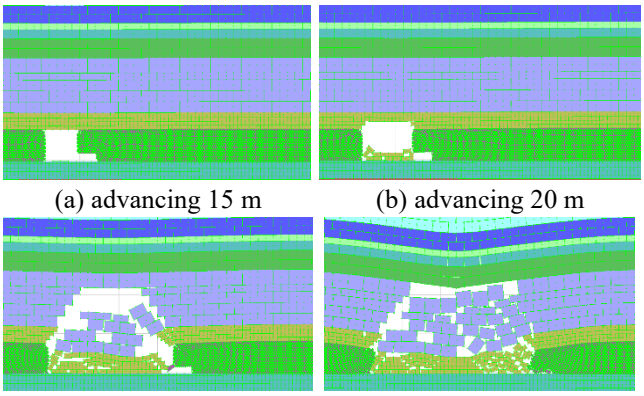

(a) advancing 15 m (b) advancing 20 m

(c) advancing 40 m (d) advancing 50 m

Fig. 25 Top-coal elastic modulus 3.29 GPa

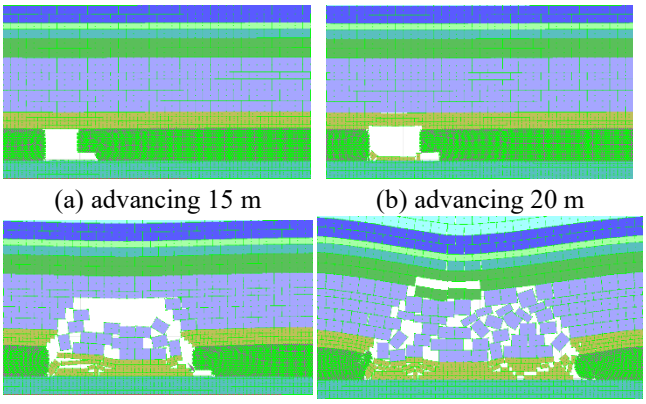

(a) advancing 15 m (b) advancing 20 m

(c) advancing 45 m (d) advancing 60 m

Fig. 26 Top-coal elastic modulus 4.42 GPa

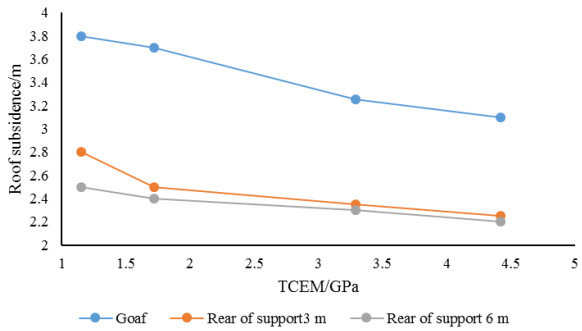

(a) Roof subsidence under initial caving

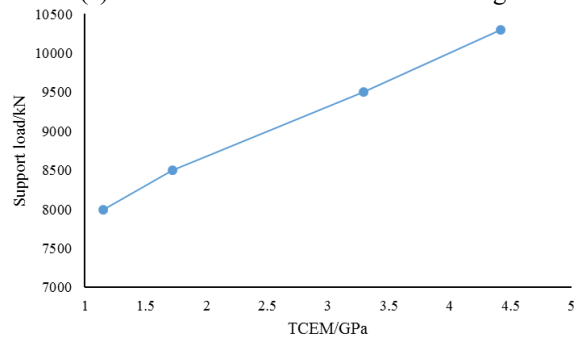

(b) Support load under initial caving

Fig. 27 Characteristics of initial weighting versus TCEM

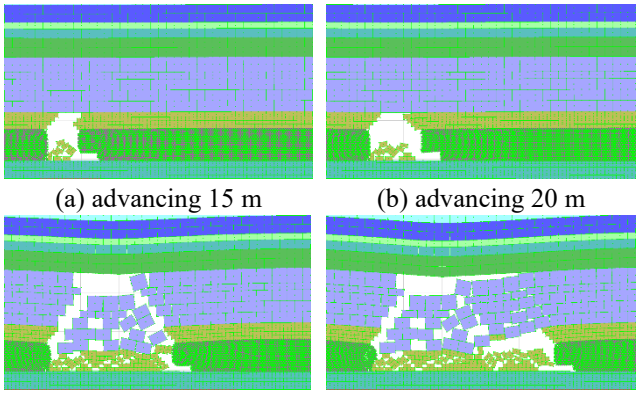

(a) advancing 15 m (b) advancing 20 m

(c) advancing 40 m (d) advancing 50 m

Fig. 28 Immediate roof elastic modulus 4.17 GPa

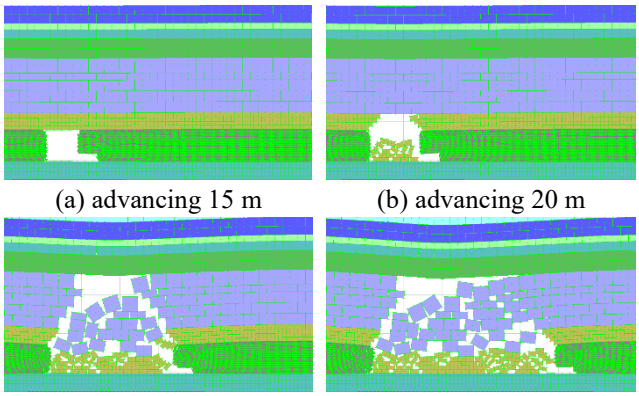

(a) advancing 15 m (b) advancing 20 m

(c) advancing 40 m (d) advancing 55 m

Fig. 29 Immediate roof elastic modulus 5.0GPa

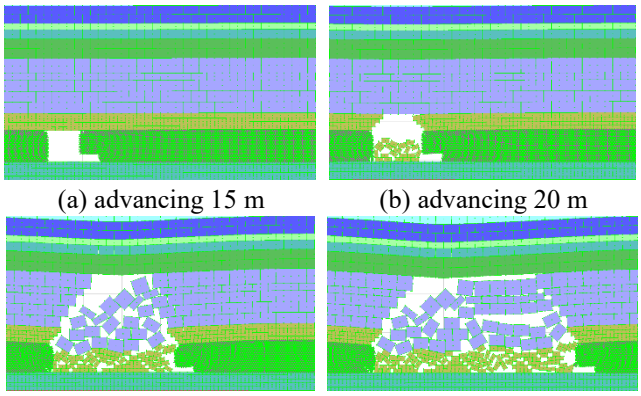

(a) advancing 15 m (b) advancing 20 m

(c) advancing 40 m (d) advancing 65 m

Fig. 30 Immediate roof elastic modulus 5.83 GPa

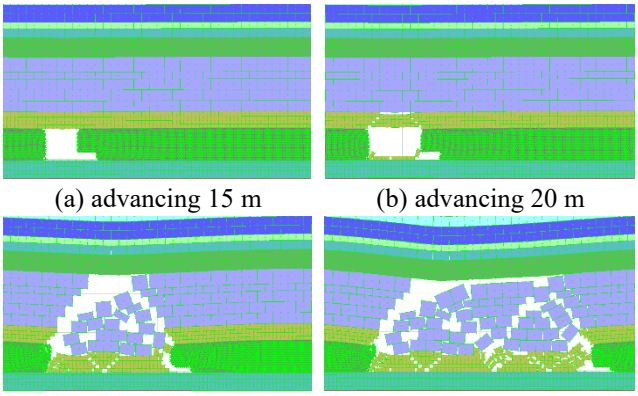

(a) advancing 15 m (b) advancing 20 m

(c) advancing 40 m (d) advancing 65 m

Fig. 31 Immediate roof elastic modulus 7.21 GPa

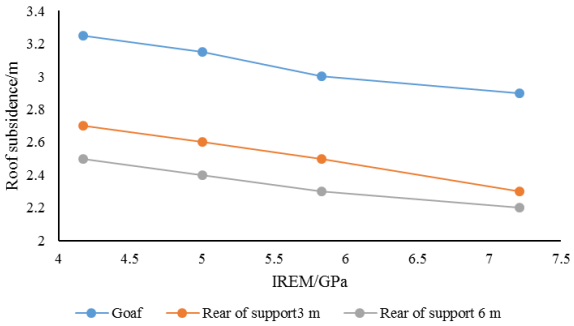

(a) Roof subsidence under initial caving

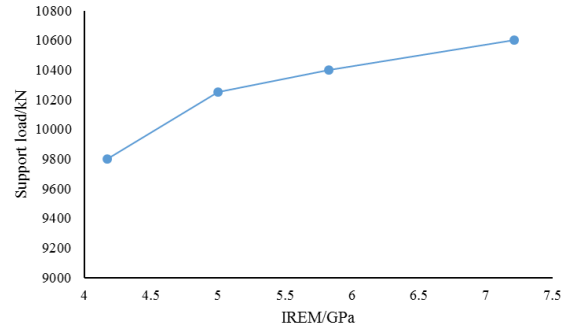

(b) Support load under initial caving

Fig. 32 Characteristics of initial weighting versus IREM

As shown in Fig. 21, the initial caving weight can be observed when the advancing distance is 35 m. And another 10 m advancing leads to the first periodic caving weight. Therefore, the initial caving distance and periodic caving

distance can be regards as 35 m and 10m with the IRT of 9 m. In general, with the increase of IRT causing mining space increasing as well, the caving distance of working face decreases.

In terms of support load and roof subsidence under the occurrence of initial caving weight with various IRT, the results of three positions in the range of roof-control distance are exhibited in Fig. 22. It can be observed that roof subsidence linear increases with the increase of IRT, while it decreases along with the advancing distance. Moreover, although support load increases as well with the increase of IRT under the occurrence of initial caving weight, the total increment value can be ignored.

4.2.3 Top-coal elastic modulus

The strata behaviors with various TCEM in TCCWF can be illustrated in Figs. 23-26. Immediate roof occurs a slight subsidence with the advancing distance of 15 m followed by collapsing directly under advancing distance reaching to 20 m when TCEM is 1.15 GPa. Moreover, when TCEM increases to 1.72 Gpa, 3.29 Gpa and 4.42 Gpa, the initial caving distance is 30 m, 40 m and 45 m, respectively. And periodic caving distance is corresponding to 10 m, 10 m and 15 m, respectively. Obviously, the increase of TCEM leads to a better integrity of coal-rock combined body for undertake more overlying loads. Thus, the caving distance can be observed a slight increasing.

The values of roof subsidence and support load are monitored under the initial caving weight as shown in Fig. 27. Obviously, roof subsidence decreases with the increase of TCEM and its decrement tends to small in the limit range of roof-control distance. At the same time, roof subsidence decreases along with the advancing direction. Moreover, support load increases with the increase of TCEM and its increment tends to small as well.

4.2.4 Immediate roof elastic modulus

As shown in Figs. 28-31, the strata behaviors with various IREM can be illustrated. To be specific, the initial caving distance is almost 40 m with the increase of IREM. However, the periodic caving distance is 10 m, 15 m, 25 m and 25 m when IREM is 4.17 GPa, 5.0 GPa, 5.83 GPa and 7.21 GPa, respectively. Similarly, the increase of IREM can also lead to a better integrity of coal-rock combined body. Therefore, although IREM has limit influence on the initial caving distance, periodic caving distance has a significant increasing with the increase of IREM.

In terms of roof subsidence and support load with various IREM under initial caving weight, the results of three positions with goaf, rear of support 3 m and rear of support 5 m can be illustrated in Fig. 32. With the increase of IREM, roof subsidence decreases along with the advancing direction and support load decreases. However, the tendency shows to become slow.

5. Conclusions

Taking Qingdong 828 working face as engineering background, two numerical simulation methods are adopted to explore the influence of coal-rock combined body properties (e.g., TCT, IRT, TCEM and IREM) on strata behaviors (e.g., vertical stress, vertical displacement, initial caving distance, periodic caving distance, roof subsidence and support resistance). Some conclusions are obtained as follow.

1) The maximum roof subsidence increases with the increase of TCT and IRT as well as the decrease of TCEM and IREM under the same advancing distance. In terms of a specific point within the roof-control distance, the roof subsidence increases with the increase of TCT and IRT as well as the decrease of TCEM and IREM. The former increment is constant while the later increment tends to slow.

2) The increase of TCT contributes to the increase of the maximum advancing support stress and the forward move of peak point causing a wide distribution, while the maximum advancing support stress decreasing and the location of peak point keeping constant can be observed with the increase of IRT. In terms of a specific point, vertical stress decreases with the increase of TCT and IRT and its decrement tends to slow. Although the maximum advancing support stress increases with the increase of TCEM and IREM, the location of peak point and distribution range have no significant change.

3) The increase of TCT and IRT leads to the decrease of caving distance because of mining space increasing. Moreover, the higher TCEM and IREM represents a better integrity of coal-rock combined body to possess better bearing capacity for overlying strata load. Therefore, caving distance increases with the increase of TCEM and IREM.

4) Roof subsidence under initial caving liner increases with the increase of TCT and IRT. And support resistance decreases with the increase of TCT and IRT along with its decrement tending to small. On the other hand, the increase of TCEM and IREM causes to the decrease of roof subsidence and its decrement tends to small, which is totally opposite to the condition of support resistance.

Acknowledgments

The authors wish to acknowledge the support from China Scholarship Council (CSC), the National Natural Science Foundation of China (No. 51674264), the National Key Research and Development Project (No. 51934008), the National Key Research and Development Plan (No. 2018YFC0604501) and the Yue Qi Distinguished Scholar Project, China University of Mining & Technology, Beijing (No. 800015Z1138). The authors would also like to thank the editors and anonymous reviewers for their valuable time and suggestions.

References

Alehossein, H. and Korinets, A. (2000), "Mesh-independent finite difference analysis using gradient-dependent plasticity", *Commun. Numer. Meth. Eng.*, **16**(5), 363-375. https://doi.org/10.1016/j.ijrmms.2004.08.007.

Alehossein, H. and Poulsen, B.A. (2010), "Stress analysis of longwall top coal caving", *Int. J. Rock Mech. Min. Sci.*, **47**(1), 30-41. https://doi.org/10.1016/j.ijrmms.2009.07.004.

Alejano, L.R., Ramirez-Oyanguren, P. and Taboada, J. (1999), "FDM predictive methodology for subsidence due to flat and inclined coal seam mining", *Int. J. Rock Mech. Min. Sci.*, **36**, 475-491. https://doi.org/10.1016/S0148-9062(99)00022-4.

Basarir, H., Oge, I.F. and Aydin, O. (2015), "Prediction of the stresses around main and tail gates during top coal caving by 3D numerical analysis", *Int. J. Rock Mech. Min. Sci.*, **76**, 88-97. https://doi.org/10.1016/j.ijrmms.2015.03.001

BP (2018), "BP Statistical review of world energy", British Petroleum, London, U.K.

Cheng, Z.B., Li, L.H. and Zhang, Y.N. (2019), "Laboratory investigation of the mechanical properties of coal-rock combined body", *Bull. Eng. Geol. Environ.* https://doi.org/10.1007/s10064-019-01613-z.

Cheng, Z.B., Zhang, Y.N., Li, L.H. and Lv, H.Y. (2018), "Theoretical solution and analysis of the elastic modulus and foundation coefficient of coal-rock combination material", *Int. J. Mater. Sci. Res.*, **1**(1), 23-31.

Guo, J., Feng, G., Wang, P., Qi, T., Zhang, X. and Yan, Y. (2018), "Roof strata behaviour and support resistance determination for ultra-thick longwall top coal caving panel: A case study of the Tashan coal mine", *Energies*, **11**(5), 1041. https://doi.org/10.3390/en11051041.

Hock, E. and Brown, E.T. (1997), "Practical estimates of rock mass strength", *Int. J. Rock Mech. Min. Sci.*, **34**(8), 1165-1186. https://doi.org/10.1016/S1365-1609(97)80069-X.

Itasca Consulting Group (2004), "UDEC2D universal distinct element code", Minneapolis, Minnesota, U.S.A.

Itasca Consulting Group (2012), "FLAC3D 5.0 Manual", Minneapolis, Minnesota, U.S.A.

Jirankova, E. (2012), "Utilisation of surface subsidence measurements in assessing failures of rigid strata overlying extracted coal seams", *Int. J. Rock Mech. Min. Sci.*, **53**, 111-119. https://doi.org/10.1016/j.ijrmms.2012.05.007.

Kirzhner, F. and Rozenbaum, M. (2001), "Behavior of the working fluid in mechanized support in permafrost", *J. Cold Reg. Eng.*, **15**(3), 170-185. https://doi.org/10.1061/(ASCE)0887-381X(2001)15:3(170).

Kong, D., Cheng, Z. and Zheng, S. (2019), "Study on failure mechanism and stability control measures in large-cutting-height coal mining face with deep-buried seam", *Bull. Eng. Geol. Environ.*, 1-15. https://doi.org/10.1007/s10064-019-01523-0.

Lei, C., Yang, J.H., Song, G.F. and Zhang, K. (2016), "Calculation of weighting interval and real-time working resistance based on beam elastic foundation method", *Electron. J. Geotech. Eng.*, **21**(5), 1931-1942.

Liu, F., Guo, Z., Lv, H. and Cheng, Z. (2018), "Test and analysis of blast wave in mortar test block", *Int. J. Rock Mech. Min. Sci.*, **108**, 80-85. https://doi.org/10.1016/j.ijrmms.2018.06.003.

Liu, X.J. and Cheng, Z.B. (2019), "Changes in subsidence-field surface movement in shallow-seam coal mining", *J. S. Afr. Inst. Min. Metall.*, **119**, 201-206. https://doi.org/10.17159/2411-9717/2019/v119n2a12.

Lv, H., Tang, Y., Zhang, L., Cheng, Z. and Zhang, Y. (2019), "Analysis for mechanical characteristics and failure models of coal specimens with non-penetrating single crack", *Geomech. Eng.*, **17**(4), 355-365. https://doi.org/10.12989/gae.2019.17.4.355.

Marschalko, M., Bednarik, M., Yilmaz, I., Bouchal, T. and Kubecka, K. (2011), "Evaluation of subsidence due to underground coal mining: an example from the Czech Republic", *Bull. Eng. Geol. Environ.*, **71**, 105-111. https://doi.org/10.1007/s10064-011-0401-8.

Masri, M., Sibai, M., Shao, J.F. and Mainguy M. (2014), "Experimental investigation of the effect of temperature on the mechanical behavior of Tournemire shale", *Int. J. Rock Mech. Min. Sci.*, **70**(9), 185-191. https://doi.org/10.1016/j.ijrmms.2014.05.007.

Pan, W., Nie, X. and Li, X. (2019), "Effect of premining on hard roof distress behavior: a case study. Rock Mechanics and Rock Engineering", *Rock Mech. Rock Eng.*, **52**(6), 1871. https://doi.org/10.1007/s00603-018-1657-0.

Sasaoka, T., Takamoto, H., Shimada, H., Oya, J., Hamanaka, A. and Matsui, K. (2015), "Surface subsidence due to underground mining operation under weak geological condition in Indonesia", *J. Rock Mech. Geotech. Eng.*, **7**(3), 337-344. https://doi.org/10.1016/j.jrmge.2015.01.007.

Schweitzer, R. (1977), "Thick seam winning methods in French coal mines", *Proceedings of the International Symposium on Thick Seam Mining*, Dhanbad, India, May.

Suchowerska, A.M., Carter, J.P. and Hambleton, J.P. (2015), "Geomechanics of subsidence above single and multi-seam coal mining", *J. Rock Mech. Geotech. Eng.*, **8**, 304-313. https://doi.org/10.1016/j.jrmge.2015.11.007.

Sun, W., Du, H., Zhou, F. and Shao, J. (2019), "Experimental study of crack propagation of rock-like specimens containing conjugate fractures", *Geomech. Eng.*, **17**(4), 323-331. https://doi.org/10.12989/gae.2019.17.4.323.

Vakili, A. and Hebblewhite, B.K. (2010), "A new cavability assessment criterion for longwall top coal caving", *Int. J. Rock Mech. Min. Sci.*, **47**(8), 1317-1329. https://doi.org/10.1016/j.ijrmms.2010.08.010.

Wang, J., Yang, S., Li, Y. and Wang, Z. (2015), "A dynamic method to determine the supports capacity in longwall coal mining", *Int. J. Min. Reclam. Environ.*, **29**(4), 277-288. https://doi.org/10.1080/17480930.2014.891694.

Wang, J., Yang, S., Li, Y., Wei, L., and Liu, H. (2014), "Caving mechanisms of loose top-coal in longwall top-coal caving mining method", *Int. J. Rock Mech. Min. Sci.*, **71**, 160-170. https://doi.org/10.1016/j.ijrmms.2014.04.024.

Xie, G.X., Chang, J.C. and Yang, K. (2009), "Investigations into stress shell characteristics of surrounding rock in fully mechanized top-coal caving face", *Int. J. Rock Mech. Min. Sci.*, **46**(1), 172-181. https://doi.org/10.1016/j.ijrmms.2008.09.006.

Xie, H., Chen, Z., and Wang, J. (1999), "Three-dimensional numerical analysis of deformation and failure during top coal caving", *Int. J. Rock Mech. Min. Sci.*, **36**(5), 651-658. https://doi.org/10.1016/s0148-9062(99)00027-3.

Xie, Y.S. and Zhao, Y.S. (2009), "Numerical simulation of the top coal caving process using the discrete element method", *Int. J. Rock Mech. Min. Sci.*, **46**(6), 983-991. https://doi.org/10.1016/j.ijrmms.2009.03.005.

Yang, T., Liu, J., Finklea, H., Lee, S., Epting, W.K., Mahbub, R., Hsu, T., Salvador, P.A., Abernathy, H.W. and Hackett, G.A. (2018), "An efficient approach for prediction of Warburg-type resistance under working currents", *Int. J. Hydrogen Energy*, **43**(32), 15445-15456. https://doi.org/10.1016/j.ijhydene.2018.06.076.

Yasitli, N.E. and Unver, B. (2005), "3D numerical modeling of longwall mining with top-coal caving", *Int. J. Rock Mech. Min. Sci.*, **42**(2), 219-235. https://doi.org/10.1016/j.ijrmms.2004.08.007.

Zhang, Y., Cheng, Z. and Lv, H. (2019). "Study on failure and subsidence law of frozen soil layer in coal mine influenced by physical conditions", *Geomech. Eng.*, **18**(1), 97-109. https://doi.org/10.12989/gae.2019.18.1.97.

CC

Notations

TCCWF top-coal caving working face

TCT top-coal thickness

IRT immediate roof thickness

TCEM top-coal elastic modulus

IREM immediate roof elastic modulus